

# Origin of the DC output voltage from a high- $T_c$ superconducting dynamo.

R.C. Mataira <sup>1</sup>, M.D. Ainslie <sup>2</sup>, R.A. Badcock <sup>1</sup> and C.W. Bumby <sup>1, a)</sup>

<sup>1)</sup> *Robinson Research Institute, Victoria University of Wellington, 69 Gracefield Road, Lower Hutt 5010, New Zealand*

<sup>2)</sup> *Bulk Superconductivity Group, Department of Engineering, University of Cambridge, Trumpington Street, Cambridge CB2 1PZ, United Kingdom*

Despite their proven ability to output DC currents of  $>100$  A, the physical mechanism which underpins the operation of a high- $T_c$  superconducting (HTS) dynamo is still widely debated. Here, we show that the experimentally observed open-circuit DC output voltage,  $V_{dc}$ , is due to the action of overcritical eddy currents within the stator wire. We demonstrate close agreement between experimental results and numerical calculations, and show that large over-critical currents flow within the high- $T_c$  stator during certain parts of the dynamo cycle. These overcritical currents experience a non-linear local resistivity which alters the output voltage waveform obtained in the superconducting state. As a result, the full-cycle integral of this altered waveform outputs a non-zero time-averaged dc voltage. We further show that the only necessary requirement for a non-zero  $V_{dc}$  output from any dynamo, is that the stator must possess a non-linear local resistivity. Here, this is provided by the flux-flow regime of a HTS coated conductor wire, where conduction is described by the  $E - J$  power law. We also show that increased values of  $V_{dc}$  can be obtained by employing stator wires which exhibit a strong in-field dependence of the critical current  $J_c(B, \theta)$ . However, non-linear resistivity is the key requirement to realize a DC output, as linear magneto-resistance is not sufficient. Our results clarify this longstanding conundrum, and have direct implications for the optimization of future HTS dynamo devices.

PACS numbers: Valid PACS appear here

The high- $T_c$  superconducting (HTS) dynamo<sup>1-3</sup>, is a device which has drawn recent attention<sup>4-16</sup>, due to its practical utility to inject large dc supercurrents into a closed superconducting circuit. These devices open the door to new types of HTS magnets which do not require bulky electronic current supplies connected through thermally inefficient metal current leads<sup>10</sup>. The resulting reduction in thermal load would enable smaller, lighter and cheaper cryogenic systems to be employed, making portable high current HTS electromagnets and machines a truly viable proposition<sup>4,14</sup>. However, despite extensive experimental study to date, the underlying physical origin of the dc output obtained from an HTS dynamo is not well understood.

The central point of confusion is that the HTS dynamo develops a DC open-circuit output from a rotating ac magnetic field, in apparent contravention of Faraday's law<sup>9,17</sup>. Several different explanations have been proposed to reconcile this issue<sup>7-9,12,15,18-20</sup>, but quantitative predictive calculations which match experimental data have proved elusive. Here we present numerical modelling calculations which closely reproduce measured transient and DC output voltages from an experimental HTS dynamo. We show that the open-circuit output voltage is well explained using classical electromagnetic theory, without invoking either exotic quantum flux-coupling mechanisms<sup>15,19</sup>, nor consideration of flux-trapping within an extended closed superconducting loop<sup>12,20</sup>. Rather, the DC output arises from a local rectification effect within the HTS stator tape<sup>7-9</sup>. This

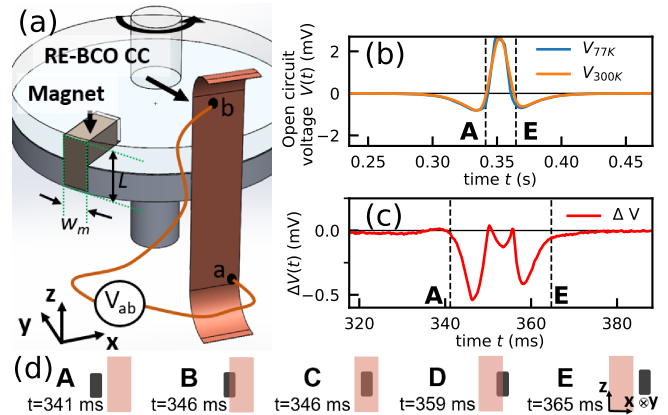


FIG. 1. (a) Schematic of the experimental HTS dynamo studied in this work. (b) Experimental open-circuit voltage waveforms measured in the superconducting ( $V_{77K}$ ) and normal-conducting ( $V_{300K}$ ) states. (c)  $\Delta V(t)$  waveform during the high field part of the cycle. (d) Key positions of the rotor magnet as it traverses the HTS stator tape.

is caused by overcritical eddy currents which flow within the HTS film during the high field part of the rotor cycle, and which incur a non-linear local resistivity.

The dynamo topology studied here is similar to that described in previous work<sup>21</sup>, and is depicted in Fig. 1(a). It consists of a rotor which houses a Nd-Fe-B magnet with an edge length,  $L$ , of 12.7 mm, and width,  $w_m$ , of 6 mm. The magnet's outer face is positioned 35 mm from the axis of rotation, with its pole facing outwards. A section of 12 mm wide ReBCO tape (Superpower SF12050CF) is oriented parallel to the axis of rotation, with its planar surface facing the rotor. The flux gap,  $g$ , between the

<sup>a)</sup>Electronic mail: chris.bumby@vuw.ac.nz

superconducting tape and the rotor magnet was 3.7 mm. A rotational frequency of 4.25 Hz was employed, with the rotor magnet traversing the tape once during each cycle. Illustrative locations of the magnet's transit across the tape are illustrated in Fig. 1 (d). Thin copper wires were mechanically fixed in place and attached as voltage taps at either end of the ReBCO tape. The entire arrangement was then placed in a liquid nitrogen cryostat. The output voltage waveform and time-averaged dc voltage were measured at both room temperature and 77 K.

The open-circuit output obtained from this device is similar to those previously reported in<sup>9</sup>. Fig. 1(b) shows the open-circuit voltage waveform measured in both the normal-conducting state at 300 K ( $V_{300K}$ ), and in the superconducting state at 77 K ( $V_{77K}$ ). The large positive peak at position C corresponds to the moment at which the rotor magnet is centred directly above the stator tape. Subtle differences between the normal and superconducting waveforms are apparent during this part of the cycle. These are highlighted in Fig. 1(c) which plots the difference:

$$\Delta V(t) = V_{77K}(t) - V_{300K}(t), \quad (1)$$

where each voltage is a function time,  $t$ .  $\Delta V$  eliminates contributions from induced emfs in the measurement leads, and hence describes only the contribution from the superconducting tape. The time averaged DC voltage output by the dynamo,  $V_{dc}$ , is given by:

$$V_{dc} = f \int_0^{\frac{1}{f}} V_{77K}(t) dt = f \int_0^{\frac{1}{f}} \Delta V(t) dt. \quad (2)$$

where  $f$  is the cycle frequency of the dynamo. The RHS of eq 2 holds, because in the normal-conducting case at 300K,  $V_{dc} = 0$ . This is expected as the dynamo geometry is that of a simple ac alternator<sup>9</sup>. However, it is clear from Fig. 1(c) that in the superconducting state at 77K,  $V_{dc} \neq 0$ . As a result, if a superconducting coil is connected in series with the dynamo, the non-zero dc output voltage will drive a dc current to flow through the coil<sup>1,5,22</sup>. An important point to note from plots Fig. 1(b) and (c) is that  $V_{dc}$  occurs in the *opposite polarity* to the voltage peak observed as the magnet crosses the tape. This means that  $V_{dc}$  actually opposes the emf caused by the traversal of applied flux across the stator wire, and hence cannot be understood in terms of a simple flux transfer model.<sup>15,20</sup> Nor can a DC output voltage arise from magnetisation effects within the HTS tape. This is because  $\mathbf{B}$ , must always be periodic over 1 cycle at all points in space, such that:

$$\int_0^{1/f} (\nabla \times \mathbf{E}) dt = - \int_0^{1/f} \frac{d\mathbf{B}}{dt} dt = 0 \quad (3)$$

Instead, we must consider the time-evolution of the electrostatic scalar potential,  $\psi$ . This has the gauge invariant form:

$$\nabla\psi = -\partial_t \mathbf{A} - \mathbf{E} = -\partial_t \mathbf{A} - \rho \mathbf{J}, \quad (4)$$

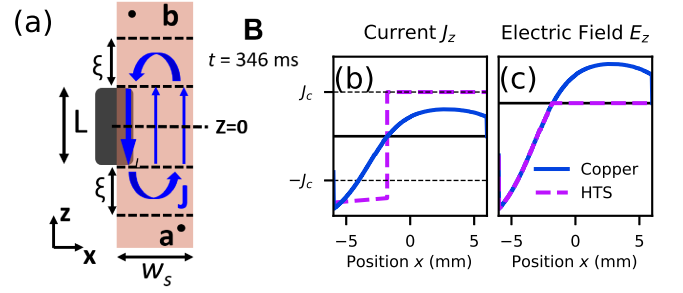


FIG. 2. (a) Schematic depiction of the circulating currents flowing in HTS tape when the rotor magnet is at position **B**. Bold arrows indicate over-critical current densities. (b)  $J_z$  profiles along the line  $z = 0$  flowing in either copper or HTS stators. (c)  $E_z = \rho J_z$  profiles corresponding to currents depicted in (b).

where  $\mathbf{A}$  is the magnetic vector potential,  $\rho$  is the local sheet resistivity, and  $\mathbf{J}$  is the local sheet current density.

The experimentally measured waveform,  $V_{ab}$  (Fig. 1(b)), is obtained from a voltmeter connected to a closed loop formed by the measurement leads and the HTS tape<sup>23</sup>. The leads connect to either end of the HTS tape at points **a** and **b**, and we denote the paths through the HTS tape and leads as  $C_s$  and  $C_l$  respectively. As no current flows within the thin measurement leads, we can express  $V_{ab}$  as the sum of the path integrals through  $C_s$  and  $C_l$ :

$$\begin{aligned} V_{ab}(t) &= \int_{C_s} \nabla\psi \cdot d\mathbf{l} + \int_{C_l} \nabla\psi \cdot d\mathbf{l} \\ &= - \int_{C_s} \rho \mathbf{J} \cdot d\mathbf{l} - \oint_{C_s + C_l} \partial_t \mathbf{A} \cdot d\mathbf{l}. \end{aligned} \quad (5)$$

It is important to note that  $\mathbf{A}$  is periodic over one cycle of the dynamo rotor and hence the time-averaged (dc) value of  $\partial_t \mathbf{A}$  must always be zero at every point in space. As such we arrive at:

$$V_{dc} = -f \int_0^{\frac{1}{f}} dt \int_{C_s} \rho \mathbf{J} \cdot d\mathbf{l}, \quad (6)$$

In the open-circuit condition there is no net transport current through the superconducting tape, but circulating eddy currents may nonetheless occur such that  $\mathbf{J} \neq 0$  at any local point. Such currents occur during dynamo operation, as flux penetrates the HTS tape<sup>22</sup> inducing eddy currents to flow in the HTS film, as is depicted in Fig. 2(a). From equation 6 we see that any open-circuit dc output must solely be due to the action of these circulating eddy currents.

Now, in the open-circuit state no net transport current flows, such that:

$$\int_{-w/2}^{w/2} J_z dx = 0, \quad (7)$$

where the integral is taken across the full width of the HTS tape,  $w$ , and  $J_z$  denotes the  $z$ -component of the sheet current density.

Points  $\mathbf{a}$  and  $\mathbf{b}$  can be placed sufficiently far from the rotor magnet that lines of constant  $z$  are at equal potential (ie  $|J| < J_c$  at all  $z$  - see fig 2(a)). This enables eq 6 to be re-expressed as:

$$V_{dc} = f \frac{f}{w} \int_0^{\frac{1}{f}} dt \int_a^b dz \int_{-w/2}^{w/2} \rho J_z dx. \quad (8)$$

If  $\rho$  is constant (as for a normal-conducting metal with linear resistivity) then substitution of eq 7 into eq 8 delivers the expected result that  $V_{dc}$  must always be zero. However if instead  $\rho$  is a function of  $J$ , then eq 8 allows that time-varying eddy currents can cause  $V_{dc} \neq 0$ . This is precisely the case which holds for the HTS dynamo.

Figure 2(a), depicts the circulating eddy currents flowing in the dynamo stator when the rotor magnet is at position B. Figure 2(b) shows the corresponding  $J_z$  profile along the line  $z = 0$  across the tape, for both the superconducting and normal-conducting cases. In the superconductor two distinct regions are observed, where eddy currents with  $|J| \geq J_c$ , flow in either the forward or reverse direction. Forward currents flow in the region directly under the magnet. Here, flux penetrates and moves through the superconductor, such that charge carriers experience a Lorentz force which drives  $|J_z| > J_c$ . (It is clear from Fig 1(c) that circulating currents  $> J_c$  must flow at this time, as  $\Delta V$  reaches a peak value of  $-500 \mu\text{V}$  at position B. If we assume this is solely due to circulating currents beneath the 12 mm long magnet, this implies an average value of  $\rho J_z > 400 \mu\text{V cm}^{-1}$ , which is well within the flux-flow region of the HTS tape). Figure 2(c) shows the resulting local internal electric field profile,  $E_z = \rho J_z$  across the tape. The *forward-current region* where  $|J_z| > J_c$  incurs a non-zero  $E_z$  that opposes the local  $\partial_t \mathbf{A}$ . However, in the *reverse-current region* outside the magnet,  $|J_z| \leq J_c$  (due to eqn 7), and hence  $E_z \approx 0$ . As a result, the average field across the full width of the tape is non-zero at this point in the cycle. This situation differs markedly from the normal (linear) conductor, where  $E_z$  is always directly proportional to  $J_z$  at all points, such that the average value of  $E_z$  across the tape must always equal zero (from eqn 7). As a result,  $\Delta V$  for a linearly resistive conductor is zero at all times. By contrast  $\Delta V$  is non-zero for the superconductor, with its value determined by the relative distribution of forward and reverse eddy currents within the tape. Furthermore, if the magnet width is less than half the tape width, the reverse current region will always be wider than the forward current region. This means that  $E_z$  will always be high in the *forward-current region*, and zero in the *reverse-current region*. As a result, the full-cycle integral,  $V_{dc}$  will also be non-zero and have the opposite polarity to the emf caused by the magnet traversing the tape.

To probe this effect in more detail, we have numerically simulated the currents flowing in the stator tape of the dynamo shown in Fig. 1 (a). A 2D finite element numerical model based on the H-formulation<sup>24-29</sup> has been employed to calculate values of  $J_z$  flowing across

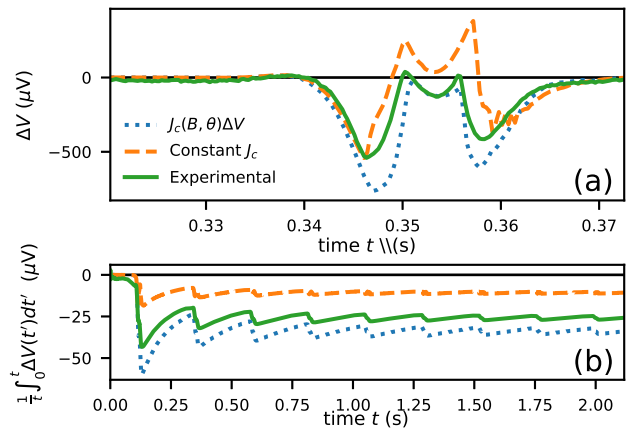


FIG. 3. (a) Plot showing comparison of experimentally-measured  $\Delta V$  alongside numerically calculated waveforms. Data shown for numerical calculations using either  $J_c = \text{const.}$ , or the experimentally determined  $J_c(B, \theta)$  function. (b) Cumulative time average,  $\frac{1}{t} \int_0^t \Delta V dt'$ , for each waveform shown above. As  $t \rightarrow \infty$  these converge to  $V_{dc}$  in each case.

the plane of symmetry at  $y = 0$  (see Fig. 2 (a)). The local resistivity within the HTS tape is described by the well-known  $E$ - $J$  power law<sup>30,31</sup>:

$$\rho = \frac{E_0}{J_c(B, \theta)^n} |J|^{n-1}, \quad (9)$$

where  $J_c(B, \theta)$  is the critical current of the HTS film in a magnetic field,  $B$ , at angle,  $\theta$  to the tape, and  $E_0$  is a constant conventionally set to  $1 \mu\text{V cm}^{-1}$ . The HTS tape used in experiments exhibited  $n = 20$ .

Values for  $\Delta V$  were calculated from the H-formulation results for copper and superconducting stators, using equations 1 and 5. This was achieved through the approximation that  $J_z$  is independent of  $z$  within the region directly beneath the rotor magnet (ie between  $z = \pm L/2$  from the model plane), and negligible at all other points (ie  $|J| \gg J_c$ ). Note that this approach assumes that the induced emf in the measurement leads is the same at both 77 K and 300 K.  $V_{dc}$  is then obtained from eq 2. Further details of the numerical simulation framework are provided in the supporting material.

Two versions of the numerical model were calculated, using different functions to describe the HTS resistivity (eq 9). In the first case,  $J_c$  was assumed to be constant and equal to  $23.6 \text{ A mm}^{-1}$ . (This is the self-field value measured at the  $1 \mu\text{V}$  criteria for the stator tape used in experiments). In the second case, values for  $J_c(B, \theta)$  and  $n$  were interpolated from experimental in-field transport measurements of the stator tape, taken between 0 - 1 T and  $0^\circ$  -  $180^\circ$  degrees<sup>32,33</sup>, with wire behaviour taken to be symmetric along  $0^\circ$ . The data is then corrected for self-field effects following the method of Zermeno et al.<sup>34</sup>.

Figure 3 shows a comparison between values calculated from the numerical model and experiment. Figure 3(a) shows good qualitative agreement in  $\Delta V$ , for both resistivity models. In each case the distinctive sequence of

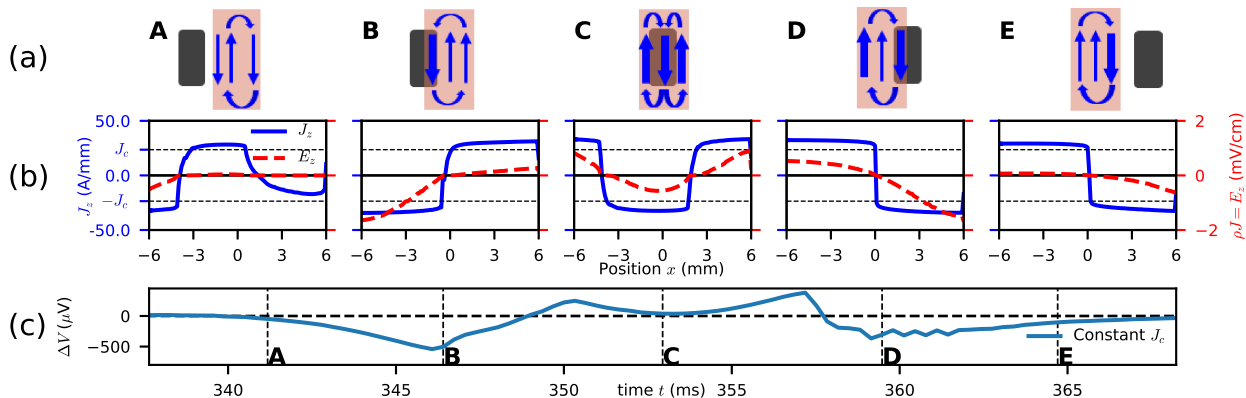


FIG. 4. (a) Schematic denoting key magnet positions A-E and the eddy currents flowing in the stator tape at each moment. (b) Calculated profiles of  $J_z$  and  $E_z = \rho J_z$  across the tape at each magnet position for the  $J_c = \text{constant}$  model (b) Calculated  $\Delta V$  waveform for the constant  $J_c$  model showing points corresponding to each profile depicted in (b) above.

quadruple peaks is observed in the  $\Delta V$  waveform, which coincide with rotor positions A to E. There is a noticeable left-to-right asymmetry in all of the experimental and calculated  $\Delta V$  waveforms, with the leading negative peak having a larger amplitude than the trailing peak in each case. This occurs because the internal field in the tape includes a contribution from the circulating currents within the superconductor. These currents switch direction as the magnet passes across the centre of the wire, causing the internal magnetic field within the tape to differ between points A and E. Similar left-to-right asymmetry also occurs in normal-conducting stator sheets carrying very large eddy currents<sup>35</sup>. However, it must be noted that this is a magnetisation effect which cannot give rise to a non-zero  $V_{dc}$  (due to eq. 3).

More detailed comparison is possible if we consider the cumulative time-averaged voltage shown in Fig 3(b). This value converges to  $V_{dc}$  as  $t \rightarrow \infty$  (experimentally measured to be  $-24.3 \mu\text{V}$ ). Fig 3(b) shows that both numerical models output a non-zero dc voltage of the correct polarity. However, whilst the  $J_c = \text{const.}$  model certainly produces a non-zero negative value for  $V_{dc}$ , this is significantly smaller than the experimental value ( $-4.03 \mu\text{V}$ ). By contrast the field-dependent  $J_c(B, \theta)$  resistivity yields a value ( $-47.8 \mu\text{V}$ ), which is comparable to experiment.

These observations indicate that the constant  $J_c$  model possesses all of the essential dynamics necessary to deliver a dc voltage. This is because the constant  $J_c$  model possesses a non-linear resistivity described by eq 9, which is all that is required for eq 8 to deliver a non-zero dc voltage. However it is also clear that consideration of  $J_c$  suppression with applied field  $B$  increases the calculated value of  $V_{dc}$ , and is needed for good agreement with experiment.

Further insight can be obtained by inspecting the currents flowing in the HTS tape. It is important to recognise that circulating currents flow within the dynamo stator wire at all times during the dynamo cycle. This

is because remanent magnetisation of the tape persists, even when the rotor magnet is at the furthest point away from the stator tape. These remanent currents exhibit  $|J| \leq J_c$ , and hence do not contribute to  $\Delta V$ . Fig. 3, clearly shows that  $\Delta V = 0$  for all times when the rotor magnet is away from the tape. However, as the rotor magnet approaches and traverses the tape, more complex dynamics occur. Fig. 5 shows the current distribution and internal field profiles at key rotor positions, with the rotor magnet moving from left to right over time. Data is shown for the  $J_c = \text{const.}$  case.

At position A, inductively-driven eddy currents with  $|J_z| \geq J_c$  are present at the left edge of the tape (closest to the magnet), whilst remanent currents from the previous rotor cycle remain at the right-hand edge of the tape (with  $|J| \leq J_c$ ). As a result the over critical currents incur a small local internal field at the left hand side of the tape, which denotes the start of the first negative peak in  $\Delta V$  (see fig. 4(c)). At position B, eddy currents flow counter-clockwise through the tape, and the situation is similar to that discussed for Fig. 2. This corresponds to the first negative peak in  $\Delta V$ . At position C, the rotor magnet is centred above the HTS tape and the forward- and reverse-current regions are approximately equal in width. As a result,  $|J_z| > J_c$  across the full width of the tape. Forward and reverse components of the internal field approximately cancel, such that  $\Delta V \approx 0$ . Position C also denotes the point at which eddy currents within the stator switch from counter clockwise to clockwise, with points D and E representing the reverse situations for B and A respectively, albeit with eddy currents now flowing in counter-rotation. Figure 4 (c), illustrates that the  $\Delta V$  waveform, emerges from the evolving average internal electric field across the tape (Fig. 4(b)). Similar current profiles are obtained for the  $J_c(B, \theta)$  case, which is given in the supplementary material. however, in this case,  $J_c$  is depressed in the high-field region beneath the magnet, meaning that overcritical currents incur larger internal electric fields than in the  $J_c = \text{constant}$  case.

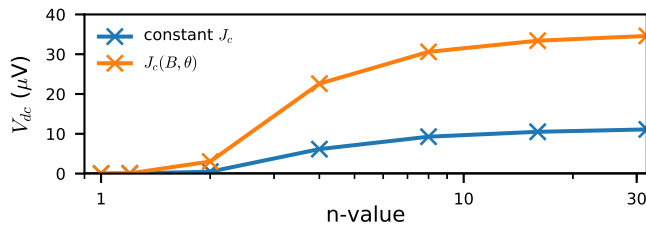


FIG. 5. Plots of  $V_{dc}$  vs  $n$ , obtained from calculations using each of the different functions for the HTS resistivity ( $J_c = const.$  or  $J_c(B, \theta)$ ).

Figure 5 shows further evidence that non-linear resistivity is the only necessary condition to obtain a non-zero  $V_{dc}$  from the dynamo. This plots calculated values of  $V_{dc}$  as a function of  $n$ -value for both the  $J_c = const.$ , and  $J_c(B, \theta)$  models. Higher values of  $n$  denote greater non-linearity in resistivity and it is clear that this leads to greater  $V_{dc}$  in both cases. Importantly we also see that when  $n = 1$  then  $V_{dc}=0$  in both cases. This means that a linear resistivity which is magnetic field dependent, is not sufficient by itself to deliver a partial rectification effect. This contradicts another previous dynamo model based on magneto-resistance, which was proposed by Giaver<sup>18</sup>.

In conclusion, we have shown that the time-averaged dc output voltage obtained from an HTS dynamo arises naturally from a local rectification effect caused by over-critical eddy currents flowing in the HTS stator sheet. This is a classical effect, and eqn 6 implies that any dynamo for which the stator comprises a material with non-linear resistivity should output a non-zero-dc voltage - although the very small eddy currents expected in a non-superconducting stator would make the effect rather difficult to measure. We also observe that a significant increase in  $V_{dc}$  can be achieved through the use of an HTS stator wire which exhibits a strong decrease in  $J_c$  under a perpendicular magnetic field. Fortuitously, such behaviour is commonly observed in thin film ReBCO coated conductors<sup>32,36</sup>, although modern commercial ReBCO wires increasingly include artificial pinning centers to counteract this effect. These ‘advanced pinning’ wires are unlikely to represent the optimal material for HTS dynamo construction.

Further details of the  $H$ -formulation model used in this work are provided in the supplementary material.

The authors wish to thank Stuart Wimbush and Bas Pellen for their help collecting  $I_c(B, \theta)$  data. MA acknowledges financial support from an EPSRC Early Career Fellowship. Additional data related to this publication is available at <https://doi.org/10.17863/CAM.33892>.

<sup>1</sup>C. Hoffmann, D. Pooke, and A. D. Caplin, IEEE Trans. Appl. Supercond. **21**, 1628 (2011).

<sup>2</sup>J. Volger and P. Admiraal, Physics Letters **2**, 257 (1962).

<sup>3</sup>H. V. Beelen, M. A. Arnold, H. Sypkens, J. V. B. Houckgeest, R. D. B. Ouboter, J. Beenakker, and K. Taconis, Physica **31**, 413 (1965).

- <sup>4</sup>R. M. Walsh, R. Slade, D. Pooke, and C. Hoffmann, IEEE Trans. Appl. Supercond. **24**, 4600805 (2014).
- <sup>5</sup>Z. Jiang, K. Hamilton, N. Amemiya, R. A. Badcock, and C. W. Bumby, Appl. Phys. Lett. **105**, 112601 (2014).
- <sup>6</sup>T. A. Coombs, J. F. Fagnard, and K. Matsuda, IEEE Trans. Appl. Supercond. **24**, 8201005 (2014).
- <sup>7</sup>J. Geng, B. Shen, C. Li, H. Zhang, K. Matsuda, J. Li, X. Zhang, and T. A. Coombs, Appl. Phys. Lett. **108**, 262601 (2016).
- <sup>8</sup>J. Geng, K. Matsuda, L. Fu, J.-F. Fagnard, H. Zhang, X. Zhang, B. Shen, Q. Dong, M. Baghdadi, and T. A. Coombs, J. Phys. D **49**, 11LT01 (2016).
- <sup>9</sup>C. W. Bumby, Z. Jiang, J. G. Storey, A. E. Pantoja, and R. A. Badcock, Appl. Phys. Lett. **108**, 122601 (2016).
- <sup>10</sup>C. W. Bumby, R. A. Badcock, H.-J. Sung, K.-M. Kim, Z. Jiang, A. E. Pantoja, P. Bernardo, M. Park, and R. G. Buckley, Supercond. Sci. Technol. **29**, 024008 (2016).
- <sup>11</sup>S. Lee, W. Kim, Y. Kim, J. Lee, S. Park, J. Lee, G. Hong, S. Kim, J. Han, Y. J. Hwang, and K. Choi, IEEE Trans. Appl. Supercond. **26**, 0606104 (2016).
- <sup>12</sup>A. M. Campbell, Supercond. Sci. Technol. **30**, 125015 (2017).
- <sup>13</sup>K. Hamilton, A. E. Pantoja, J. G. Storey, Z. Jiang, R. A. Badcock, and C. W. Bumby, IEEE Trans. Appl. Supercond. **28**, 5205705 (2018).
- <sup>14</sup>H. Jeon, J. Lee, S. Han, J. H. Kim, C. J. Hyeon, H. M. Kim, H. Kang, T. K. Ko, and Y. S. Yoon, IEEE Trans. Appl. Supercond. **28**, 5207605 (2018).
- <sup>15</sup>W. Wang and T. Coombs, Phys. Rev. Applied **9**, 044022 (2018).
- <sup>16</sup>J. Ma, J. Geng, J. Gawith, H. Zhang, C. Li, B. Shen, Q. Dong, J. Yang, J. Chen, Z. Li, and T. A. Coombs, IEEE Trans. Appl. Supercond. , 8663420 (2019).
- <sup>17</sup>M. Faraday, Phil. Trans. R. Soc. Lond **122**, 125 (1832).
- <sup>18</sup>I. Giaever, IEEE Spectr. **3**, 117 (1966).
- <sup>19</sup>V. Kaplunenko, S. Moskvina, and V. Schmidt, Fizika Nizkikh Temperatur **11**, 846 (1985).
- <sup>20</sup>L. van de Klundert and H. ten Kate, Cryogenics **21**, 195 (1981).
- <sup>21</sup>R. A. Badcock, S. Phang, A. E. Pantoja, Z. Jiang, J. G. Storey, H. Sung, M. Park, and C. W. Bumby, IEEE Trans. Appl. Supercond. **27**, 5200905 (2017).
- <sup>22</sup>Z. Jiang, C. W. Bumby, R. A. Badcock, H.-J. Sung, N. J. Long, and N. Amemiya, Supercond. Sci. Technol. **28**, 115008 (2015).
- <sup>23</sup>J. R. Clem, Physics Reports **75**, 1 (1981).
- <sup>24</sup>Z. Hong, A. M. Campbell, and T. A. Coombs, Supercond. Sci. Technol. **19**, 1246 (2006).
- <sup>25</sup>M. D. Ainslie, C. W. Bumby, Z. Jiang, R. Toyomoto, and N. Amemiya, Supercond. Sci. Technol. **31**, 074003 (2018).
- <sup>26</sup>F. Sass, G. Sotelo, R. de Andrade Junior, and F. Sirois, Supercond. Sci. Technol. **28**, 125012 (2015).
- <sup>27</sup>F. Grilli, E. Pardo, A. Stenvall, D. Nguyen, W. Yuan, and F. Gomory, IEEE Trans. Appl. Supercond. **24**, 8200433 (2014).
- <sup>28</sup>J. Geng and T. A. Coombs, Supercond. Sci. Technol. **31**, 125015 (2018).
- <sup>29</sup>V. M. R. Zermeño, A. B. Abrahamson, N. Mijatovic, B. B. Jensen, and M. P. Srensen, J. Appl. Phys. **114**, 173901 (2013).
- <sup>30</sup>J. Rhyner, Physica C **212**, 292 (1993).
- <sup>31</sup>C. Plummer and J. Evetts, IEEE Trans. Magn. **23**, 1179 (1987).
- <sup>32</sup>S. C. Wimbush and N. M. Strickland, IEEE Trans. Appl. Supercond. **27**, 8000105 (2017).
- <sup>33</sup>N. M. Strickland, C. Hoffmann, and S. C. Wimbush, Rev. Sci. Instr. **85**, 113907 (2014).
- <sup>34</sup>V. M. R. Zermeño, K. Habelok, M. Stepień, and F. Grilli, Supercond. Sci. Technol. **30**, 034001 (2017).
- <sup>35</sup>S. Bilicz, Period. Polytech. Elec. Eng. Comp. Sci. **59**, 43 (2015).
- <sup>36</sup>L. Civale, B. Maiorov, A. Serquis, J. O. Willis, J. Y. Coulter, H. Wang, Q. X. Jia, P. N. Arendt, J. L. MacManus-Driscoll, M. P. Maley, and S. R. Foltyn, Appl. Phys. Lett. **84**, 2121 (2004).

## Supplementary Materials I .

### A. Modelling Methodology

We have used a 2D finite element model to solve Faraday's equation

$$\nabla \times \mathbf{E} = -\mu_0 \frac{\partial \mathbf{H}}{\partial t}, \quad (\text{SI. 1})$$

and Ampere's equation,

$$\nabla \times \mathbf{H} = \mathbf{J}, \quad (\text{SI. 2})$$

in the case of a HTS dynamo. We solve these equations using a the  $H$ -formulation (implemented in COMSOL), which solves for  $\mathbf{H}$  directly. A constitutive relation is also needed, in order to link  $E$  and  $J$ . This is given by eq 9 for the HTS stator at 77 K, whilst at 300K the conductivity is dominated by the copper stabilising layer upon the tape ( $\rho_{Cu} = 0.19\mu\omega * cm$ ). Values for  $\Delta V$  were then calculated from the H-formulation results for both copper and superconducting stators, as

$$\Delta V(t) \approx L \int_0^w dx [\rho_{77K} \mathbf{J}_{77K} - \rho_{300K} \mathbf{J}_{300K} + \partial_t (\mathbf{A}_{77K} - \mathbf{A}_{300K})] \quad (\text{SI. 3})$$

Figure 1 shows a 3D schematic of the device, including the bisecting plane corresponding to the geometry of the finite element model. The actual geometry employed in the numerical model, which is two dimensional, is shown in Fig. SI. 1. The model is split into 3 separate domains, the rotor domain  $\Omega_R$ , the air domain  $\Omega_A$ , and the HTS domain  $\Omega_T$ , with  $x, y$  in plane and  $z$  out of plane. In order

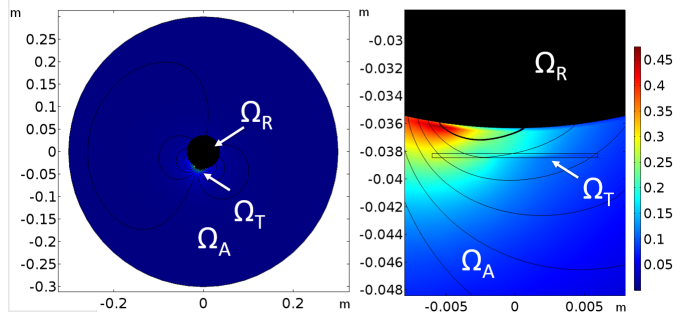


FIG. SI. 1. Snapshot of the numerical model at position  $\mathbf{A}$  including the magnitude of the magnetic field  $\mathbf{B}$ . The field in domain  $\Omega_R$  lies outside the defined boundary conditions and hence is not shown. (a) The total modelling domain, showing the rotor domain  $\Omega_R$ , the air domain  $\Omega_A$ , and the HTS domain  $\Omega_T$ . (b) A magnified view of the superconducting tape domain,  $\Omega_T$ .

to reduce computation time, the HTS domain is modelled as a  $100 \mu\text{m}$  thick film (rather than the true  $1.7 \mu\text{m}$ ). This approximation is standard practice<sup>25,29</sup>, and in this case its accuracy was confirmed through comparison with a

limited number of simulations performed using a much thinner tape domain of  $\sim 10 \mu\text{m}$ . The sheet currents  $J_z$  presented in the text are calculated as the integrals of the current density ( $\text{A}/\text{mm}^3$ ) through the depth of the domain  $\Omega_T$ . The rotor magnet field was represented in the model using a shell current on the edge of the rotor domain  $\Omega_R$ , which was rotated at the appropriate speed corresponding to  $f = 4.25 \text{ Hz}$ . This equivalently reproduces the field of the magnet in domains  $\Omega_T$  and  $\Omega_A$ . Each numerical simulation was run for 10 full cycles to ensure periodicity, and all computed values were fully periodic after the first cycle. Reported results are all from the second cycle of the simulation.

### B. $I_c(B, \theta)$ measurements for coated conductor stator wire

Fig. SI. 2 shows the measured  $I_c(B, \theta)$  for the REBCO coated conductor wire (Superpower SF12050CF) used in the experiment. This data was collected using the technique and instruments described in<sup>33</sup> and<sup>32</sup>.

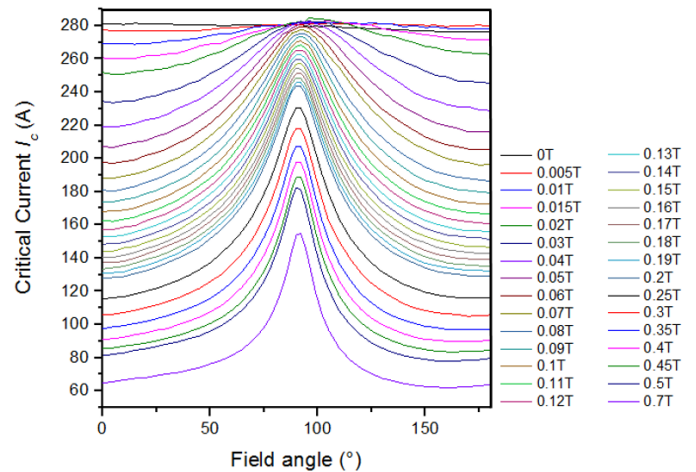


FIG. SI. 2. Experimental  $I_c(B, \theta)$  data used in the  $H$ -formulation model. Data was measured at 77.5 K in magnetic fields up to 0.7 T from a short sample of SuperPowers SF12050CF wire. The  $J_c(B, \theta)$  data is corrected for self-field using the technique presented in<sup>34</sup> and input into the model using a two-variable, direct interpolation<sup>25</sup>

### C. $J_c(B, \theta)$ current and field profiles

The  $J_c(B, \theta)$  model produces a higher output voltage as shown in Fig. 3 (a). Fig. SI. 3 shows how suppression of  $J_c$  under the magnet allows more forward over-current to be returned over a smaller region of higher  $J_c$ , this effect acts in the same direction as the effect described in the text, but is, by itself, not capable of giving the DC output, as argued in Fig. 5.

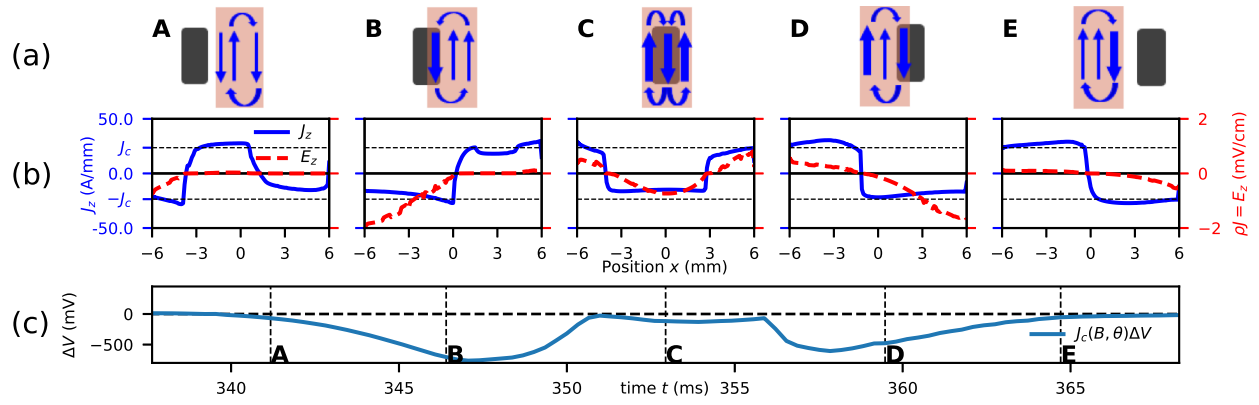


FIG. SI. 3. (a) Schematic denoting key magnet positions A-E and the eddy currents flowing in the stator tape at each moment. (b) Calculated profiles of  $J_z$  and  $E_z = \rho J_z$  across the tape at each magnet position for the  $J_c = \text{constant}$  model (b) Calculated  $\Delta V$  waveform for the  $J_c(B, \theta)$  model showing points corresponding to each profile depicted in (b) above.